Article

Design and Optimization of a Compact Super-Wideband MIMO Antenna with High Isolation and Gain for 5G Applications

Bashar A. F. Esmail [1,2], Slawomir Koziel [1,3] and Anna Pietrenko-Dabrowska [3,*]

1 Department of Engineering, Reykjavik University, 102 Reykjavík, Iceland; basharf@ru.is (B.A.F.E.); koziel@ru.is (S.K.)
2 Department of Electrical & Computer Engineering, University of Manitoba, Winnipeg, MB R3T 5V6, Canada
3 Faculty of Electronics, Telecommunications and Informatics, Gdansk University of Technology, 80-233 Gdansk, Poland
* Correspondence: anna.dabrowska@pg.edu.pl

Abstract: This paper presents a super-wideband multiple-input multiple-output (SWB MIMO) antenna with low profile, low mutual coupling, high gain, and compact size for microwave and millimeter-wave (mm-wave) fifth-generation (5G) applications. A single antenna is a simple elliptical-square shape with a small physical size of $20 \times 20 \times 0.787$ mm^3. The combination of both square and elliptical shapes results in an exceptionally broad impedance bandwidth spanning from 3.4 to 70 GHz. Antenna dimensions are optimized using the trust-region algorithm to enhance its impedance bandwidth and maintain the gain within a predefined limit across the entire band. For that purpose, regularized merit function is defined, which permits to control both the single antenna reflection response and gain. Subsequently, the SWB MIMO system is constructed with four radiators arranged orthogonally. This arrangement results in high isolation, better than 20 dB, over a frequency band from 3.4 to 70 GHz band. Further, the system achieves an average gain of approximately 7 dB below 45 GHz and a maximum gain equal to 12 dB for 70 GHz. The system exhibits excellent diversity performance throughout the entire bandwidth, as evidenced by the low envelope correlation coefficient (ECC) ($<3 \times 10^{-3}$), total active reflection coefficient (TARC) (≤ -10 dB), and channel capacity loss (CCL) (<0.3 bit/s/Hz) metrics, as well as the high diversity gain (DG) of approximately 10 dB. Experimental validation of the developed SWB MIMO demonstrates a good matching between the measurements and simulations.

Keywords: 5G; MIMO; parameter tuning; SWB; trust-region gradient-based optimization

1. Introduction

Over the years, the telecommunication industry has experienced a rapid growth due to the emergence of advanced technologies in wireless communication. To comply with the network and data traffic requirements, the fifth-generation (5G) technology has been deployed, providing broad bandwidth and data rates as high as multi-gigabits per second (Gbps) [1,2]. In 5G technology, various frequency bands are employed across both microwave and millimeter-wave (mm-wave) spectra. A band of 3.5 GHz is utilized at sub-6 GHz with an enhanced bandwidth compared to the existing 4G bands [3]. The mm-wave bands at 26, 28, 38, 50, and 60 GHz offer higher data rates than sub-6 GHz bands, mainly due to their wider bandwidth [4–6]. The 5G networks enable vital technologies for deploying the Internet of Things (IoT). Consequently, it is crucial for IoT devices to be 5G-compliant [7]. To achieve this, cost-effective, compact-sized, high-gain, and efficient antennas with broad bandwidth are essential [8].

Ultra-wideband (UWB) radio technology has gained significant attention for its low power consumption and high data rate, making it suitable for numerous applications.

However, low radiation power imposes certain limitations on UWB technology in long-range communications [9]. Recently, SWB antennas have gained attention for their ability to cover both long- and short-distance communications. They can be designed to provide an extensive bandwidth ($\geq$10:1 BW ratio), which can cover nearly all candidate bands for 5G applications [10].

Various antenna designs using different techniques to enhance their bandwidth have been studied to attain an SWB property. However, these techniques typically make the SWB property more difficult and time-consuming to achieve, and the resulting antenna structures tend to be bulky. To save time and resources, employing optimization methods may yield an extremely wide frequency range with less effort and in a shorter timeframe. The authors of [11] proposed a modified bow-tie antenna with the aim of achieving a high impedance bandwidth that spans from 3.035 to 17.39 GHz. The structure was fed by a coplanar waveguide (CPW), which was proposed as a means of enhancing the impedance bandwidth. However, the antenna size was somewhat bulky, and there was room for further improvement of its impedance bandwidth. Utilization of a triple elliptical patch was proposed in [12] to achieve a wide bandwidth range of 2.11−70 GHz. To enhance the bandwidth, a defected ground structure (DGS) was employed. Notwithstanding, the antenna structure was somewhat large and the DGS technique added complexity to the system. Furthermore, Ullah et al. [13] employed DGS to enhance the s-shaped monopole antenna and achieve SWB within the range of 3.08−40.9 GHz. The authors of [14] introduced a bulb-shaped monopole antenna with an added layer of frequency selective surface (FSS) to achieve SWB and a maximum gain of 7.16 dBi within the 3−35.92 GHz range. Nonetheless, the antenna size was large due to the addition of the FSS layer. A monopole antenna, designed to attain a bandwidth of 28.2 GHz (spanning from 1.8 to 30 GHz), was presented by Lazovic et al. in [15].

MIMO technology is utilized to improve link quality by increasing multiplexing gain and diversity. Further, it is employed to mitigate multipath fading [16]. Merging MIMO and SWB technologies can provide substantial benefits for communication systems. However, there are only a few reports in the literature that discuss SWB MIMO structures. The authors of [17] introduced a four-element SWB MIMO antenna designed to achieve a high isolation of 17 dB within the 3−40 GHz range. The spade-shaped design formed a single antenna with physical dimensions of $29 \times 22 \times 1$ mm^3. To enhance the isolation, a windmill-shaped structure was added, which increased the design complexity. A four-port SWB MIMO system, which operated between 1.37−16 GHz, was constructed using a Yagi antenna with dimensions of $45 \times 55 \times 1.6$ mm^3 [18]. A proper arrangement of the MIMO radiators enabled the system to provide a low coupling of less than −16 dB. Despite managing to attain an acceptable level of isolation without decoupling structures, the system was bulky. Additionally, further improvement in bandwidth was necessary to meet the requirements of modern wireless communication trends, including the 5G bands. The study conducted in [19] analyzed the isolation performance of a dual-port MIMO system built with a feather-shaped antenna, which was found to exceed 15 dB across the frequency range of 4.4−51.5 GHz. The diagonal metallic strip was placed between the two MIMO elements for mutual coupling reduction. Meeting the latest wireless network trends demands a SWB MIMO system that exhibits high isolation and gain, compact dimensions, and minimal complexity. In spite of the availability of other 3D ultra-wideband solutions with high flat-gain, such as the quadruple-ridged flared horn (QRFH) [20], Dyson quad-spiral array (DYQSA) [21], and Eleven [22], capable of efficiently supporting MIMO 5G applications, these options are discarded here due to their bulky size and intricate manufacturing. This drawback would be exacerbated, particularly if there is a requirement to extend the higher band towards the SWB range. Hence, the emphasis will be placed on planar structures to achieve a streamlined and compact system.

This paper introduces a miniaturized MIMO antenna system with low mutual coupling, high gain, and an extremely-wide impedance bandwidth. A single elliptical-square shape was used to achieve the SWB property, and the structure dimensions were optimized using a trust-region algorithm to enhance the impedance bandwidth. The four-port SWB MIMO system was then constructed and analyzed. The results demonstrate its exceptional

performance in terms of SWB (3.4−70 GHz), high gain (maximum of 12 dB), and low mutual coupling (<−20 dB). The system covers various wireless communication bands, including 5G sub-6 GHz, K/Ku-band, and 5G mm-wave. Upon manufacturing and testing the system, the simulation results were verified, and its real-world performance was assessed. The contributions of this work are summarized as follows:

I.   Designed a compact antenna with a simple structure to attain both SWB and high gain performance;
II.   An innovative optimization technique was employed to achieve an exceptionally wide bandwidth spanning from 3.4 to 70 GHz, with peak gain reaching 12 dB at 70 GHz. This optimization method employed a gradient-based algorithm with numerical derivatives and design-goal regularization to simultaneously optimize the structural dimensions, achieving both SWB and high gain, all while maintaining a low profile and compact size of $20 \times 20 \times 0.787$ mm^3;
III.   Implemented an orthogonal arrangement of a four-port SWB MIMO antenna to achieve isolation exceeding 20 dB and outstanding diversity performance, all without the need for any decoupling techniques.

The system exhibited a remarkable level of isolation and gain, while retaining a compact size and minimal complexity, surpassing the state-of-the-art structures. As the IoT and 5G technologies continue to shape smart cities, the SWB MIMO system developed in this study has promising applications in various areas including intelligent medical treatment, household and street management, energy management, and environmental well-being.

2. SIW-Based Series-Fed Dipole

A simple monopole antenna based on the elliptical-square shape is proposed in this work to achieve a super-wide operating frequency band. The design steps of the developed SWB antenna, as well as its configuration, are shown in Figure 1. The antenna was printed on a low-loss Rogers RT5880 substrate, which had a dielectric constant of 2.2, a tangent loss of 0.0009, and a thickness of 0.787 mm. The metallic copper layer had a thickness of 0.0175 mm. The initial stage involved selecting an elliptical patch that provided a broad frequency range, as shown in Figure 1a. A partial ground was incorporated to guarantee a wide impedance bandwidth [23]. Additionally, a rectangular notch measuring 2×1 mm^2 was created on the ground plane to serve the same purpose [24]. The design generated three frequency bands with broad impedance bandwidths, two below 20 GHz, and one above 41 GHz, namely 6.5−11.2 GHz, 12.8−19.7 GHz, and 41.7−70 GHz, as depicted by the reflection characteristics (marked as Step 1 in Figure 2). Afterwards, a square shape was integrated into the center of the elliptical shape to enhance the bandwidth, as depicted in Figure 1b. The inclusion of the square shape resulted in broadening the bandwidth below 20 GHz (3.6–19.7 GHz) and above 33 GHz (33.2–70 GHz), as illustrated in Figure 2 (Step 2).

Although the elliptical-square shape offered two broad impedance bandwidths, rigorous optimization could further enhance the response and provide the SWB property. However, this process requires numerous EM simulations, which can be time-consuming and also requires human intervention after each simulation. Numerical optimization can help reduce the time necessary to adjust the structure dimensions. Since the antenna response often relies on appropriate refinement of its parameters and there exist no precise formulas for designing all antenna structures, implementing optimization methods is the most effective approach to achieve the desired outcome with less time and effort. This work utilized the trust-region local optimization procedure to identify optimal antenna dimensions and improve the impedance bandwidth. The details of the optimization process can be found in Section 3.
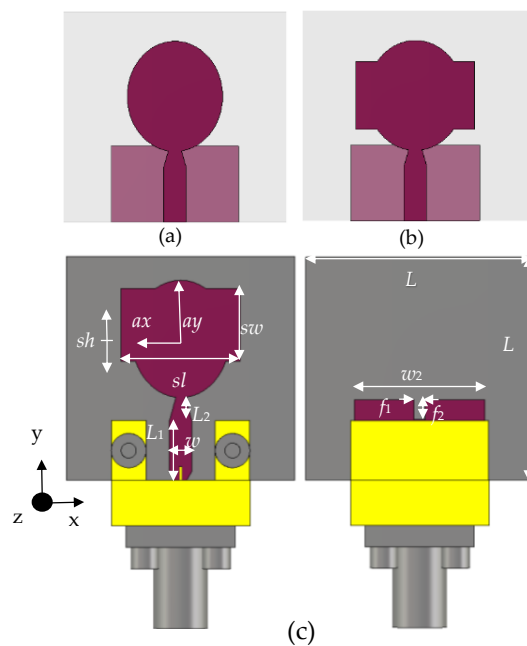
Figure 1. Configuration of the proposed SWB antenna, (**a**) Step 1, (**b**) Step 2 before optimization, (**c**) the proposed antenna geometry after optimization. The antenna dimensions are L = 20 mm, ax = 4.186 mm, ay = 5.599 mm, sl = 10.917 mm, sw = 6.363 mm, L_1 = 5.5 mm, L_2 = 3.501 mm, w = 2.1 mm, w_2 = 12 mm, f_1 = 1 mm, f_2 = 2 mm, and sh = 1.499 mm.
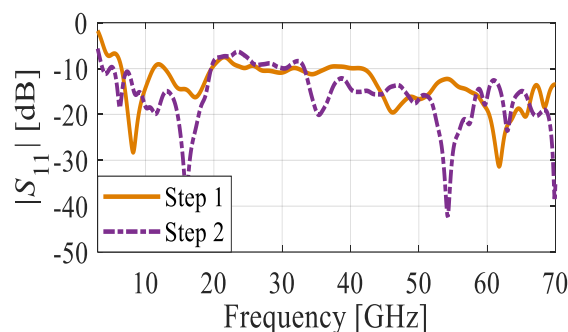

Figure 2. Reflection coefficients of the SWB antenna evaluation steps. Step 2 presents the S_{11} results before optimization.

3. SWB Performance Optimization

The major objective of the design process was to ensure impedance matching of the antenna over the frequency range $3.4 \leq f \leq 70$ GHz (covering the 5G microwave and mm-wave bands), more specifically, to fulfill the condition $|S_{11}(\boldsymbol{x}, f)| \leq -10$ dB for all $f \in F = [3.4\ 70.0]$ GHz, where $\boldsymbol{x}$ is a vector of adjustable parameters. Interactive manipulation of antenna geometry parameters using parameter sweeping or similar methods is not capable of identifying the optimum design, partly due to variable interactions, but also due to a very-broad range of operating frequencies to be controlled. In this paper, a rigorous numerical optimization was applied instead as outlined below. The designable parameters selected for the optimization process were gathered into a parameter vector $\boldsymbol{x} = [ay\ ax\ sl\ sw\ L_2\ sh]^T$, and all explained in Figure 1c. The search process was conducted over the design space X, demarked by the lower and upper bounds on the variables: $4 \leq ax$, $ay \leq 6$ mm, $9 \leq sl \leq 14$ mm, $5 \leq sw \leq 7$ mm, $2 \leq L_2 \leq 4$ mm, and $-3 \leq sh \leq 3$ mm. Furthermore, the following geometry constraints were to be satisfied: $ax < ay$ (to ensure that the major antenna axis was oriented towards the y-direction), $sl > 2ax$ (to ensure that the radiator was beyond a trivial elliptical shape), $sw < 2ay$ (to ensure that the radiator shape was not purely square), and $-(ay - sw/2) < sh < (ay - sw/2)$. The reason

for introducing the last constraint is as follows. The midpoint of the square coincides with the center of the elliptical shape and it can be vertically adjusted using *sh*. It should be noted that this movement does not exceed the *y*-axis dimension of the elliptical shape. There is also an additional constraint concerning the field properties of the antenna, namely, a requirement that the gain $G(x,f) \geq 5$ dB for $f \in F$. Given the primary objective and the constraints, the merit function undergoing minimization is formulated as follows

$$U(x) = \max_{f \in F}\{|S_{11}(x,f)|\} + \beta\left[\frac{\max\{5 - G_{\min}(x), 0\}}{5}\right]^2 \tag{1}$$

where

$$G_{\min}(x) = \min_{f \in F}\{G(x,f)\} \tag{2}$$

is the minimum in-band gain. The optimum solution x^* is the identified by solving a nonlinear minimization task

$$x^* = \arg\min_{x \in X} U(x) \tag{3}$$

Reducing the value of $U(x)$ corresponds to improving the impedance matching, as well as enforcing the condition imposed upon the antenna gain. The second term in (1) is proportional to a relative violation of the condition $G(x,f) \geq 5$ dB, with the proportionality coefficient β [25] set to 100. With this value, violations larger than a fraction of dB will result in considerable contribution of the penalty term to U, thereby fostering design relocation towards designs that satisfy that condition. At this point, it should be emphasized that implicit handling of the gain-related constraint [26] is recommended because it is a computationally-expensive one (requires EM simulation to be evaluated). The underpinning optimization engine is the trust-region (TR) algorithm [27]. The Jacobian matrix of the antenna response is evaluated by means of finite differentiation [28]. The TR algorithm produces a series $x^{(i)}$, $i = 0, 1, \ldots$, of approximations to x^* as

$$x^{(i+1)} = \max_{\substack{x \in X \\ ||x - x^{(i)}|| \leq d^{(i)}}} U_L^{(i)}(x) \tag{4}$$

In (4), $U_L^{(i)}$ is the objective function defined as in (1) but computed based on the first-order linear approximation model of antenna responses. For example, for the reflection response, we have

$$L_{S_{11}}^{(i)}(x) = S_{11}(x,f) + \nabla S_{11}(x^{(i)}, f) \cdot (x - x^{(i)}) \tag{5}$$

where $\nabla S_{11}(x^{(i)},f)$ is the gradient of the reflection response at design $x^{(i)}$ and frequency f. The linear model for the gain characteristics was defined in a similar manner. The size $d^{(i)}$ of the search region was set at the beginning of each algorithm iteration using standard TR rules [27]. The optimization was concluded when converging in argument ($||x^{(i+1)} - x^{(i)}|| < \varepsilon$; here, $\varepsilon = 10^{-3}$). The starting design $x^{(0)} = [5.5\ 4.5\ 11.0\ 6.0\ 2.8\ 0.0]^T$ was established by means of interactive parametric studies. The final (optimized) design was found to be $x^* = [5.599\ 4.186\ 10.917\ 6.363\ 3.501\ 1.499]^T$ mm. It should be noted that the optimization algorithm was implemented as an external procedure written in Matlab (Matlab 9.0.0.341360 (R2016a)). Such an implementation was much more flexible than the built-in CST (CST Studio Suite 2019) algorithms and, in particular, it allowed for a straightforward and easy control over all components of the optimization process. This was especially pertinent to the constrained objective function (1), which cannot be implemented using the built-in optimization capabilities of the simulation software. The connection between Matlab and CST was realized using Visual Basic scripts, which were used to modify the values of design parameters (as requested by the optimization engine) within the antenna project, initiate batch-mode simulation, as well as acquire and post-process

the results. Figure 2 (Step 2) and 3 show the antenna responses at the optimal and initial points. The optimized antenna exhibits an SWB spanning from 3.4 to 70 GHz and a gain exceeding 5 dB, cf. Figure 3. The radiation efficiency of the SWB antenna is depicted in Figure 3b, revealing that the average radiation efficiency of the examined antenna stood at 70.6%, with a peak efficiency reaching 86.2%.
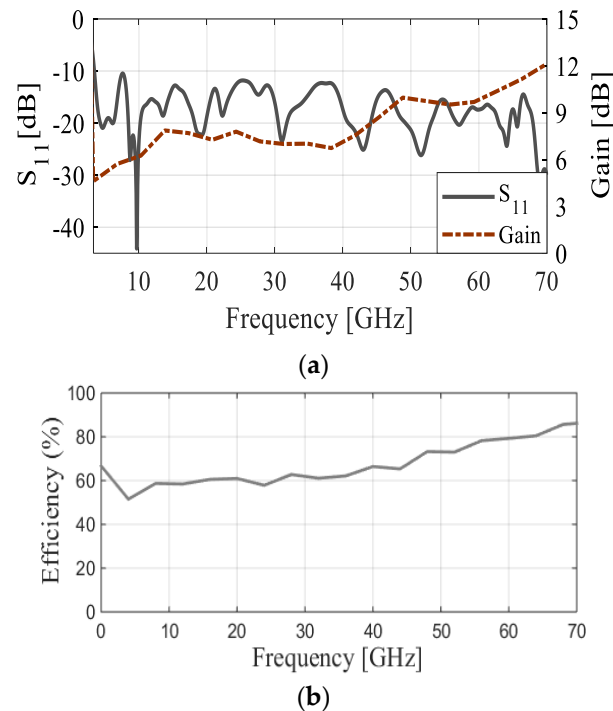

(a)

(b)

Figure 3. The SWB antenna performance, (**a**) the reflection coefficient and gain, and (**b**) the efficiency.

4. SWB MIMO Antenna Design

As mentioned earlier, MIMO technology has the potential to enhance communication systems by improving the link quality and mitigating the effects of multipath fading. When combined with the SWB property, this technology can improve communication systems even further. In this section, we present a SWB MIMO antenna, which consists of four SWB elements arranged in an orthogonal configuration. This arrangement provides high isolation across the entire bandwidth and excellent diversity performance compared to a series arrangement or even an opposite orientation. It can mitigate the limitations of both the series and opposite orientations, where the spacing between the ground planes is sufficient to prevent high mutual coupling, and where the patches are adequately spaced to enhance the overall isolation of the system. The CST-Microwave Studio-2019 was used to simulate the SWB MIMO system with a hexahedral mesh accuracy of -40 dB. Figure 4 illustrates the proposed system configuration, which was implemented on a Rogers substrate with compact dimensions of $40 \times 40 \times 0.787$ mm^3. Figure 5 shows the simulated reflection and transmission coefficients, here, presented for S_{11}, S_{21}, S_{31}, and S_{41} only due to the antenna symmetry. Although MIMO systems have multiple elements, their reflection coefficients behave similarly to that of a single-element antenna. As a result, MIMO systems can offer a wide range of frequencies, ranging from $3.4-70$ GHz. On the other hand, the MIMO elements' orthogonal configuration improves their isolation, resulting in S_{21}, S_{31}, and S_{41} magnitudes of less than -20 dB across the entire frequency range, as illustrated in Figure 5. The system achieved these properties without utilizing any decoupling techniques that could have increased its size and complexity. Through an analysis of the surface current distribution of the four SWB MIMO antenna elements, it was possible to explain their low mutual coupling. The system components are identified as Antenna 1, 2, 3, and 4. Figure 6 displays the simulated current distributions at 28 GHz, with

the excitation at Port 1 and the remaining ports terminated by a 50-Ω load. It is noteworthy that mutual coupling among the antenna elements was low, with the current concentrated at Port 1 and negligible at the remaining ports. The analysis indicates that the antennas have minimum interaction with each other.
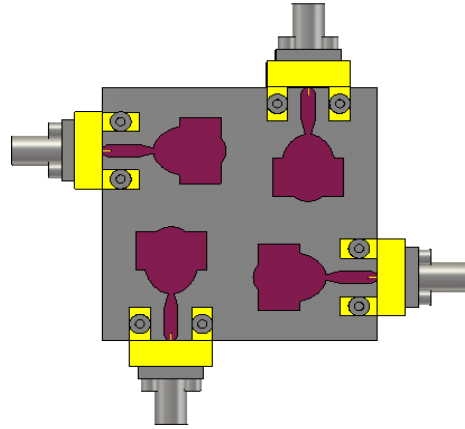

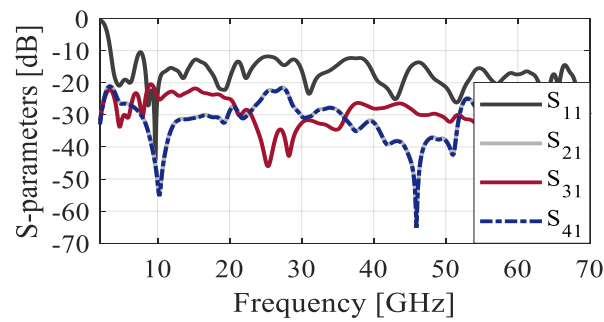
Figure 4. Configuration of the developed SWB MIMO system.

Figure 5. SWB MIMO antenna: simulated reflection and transmission characteristics.
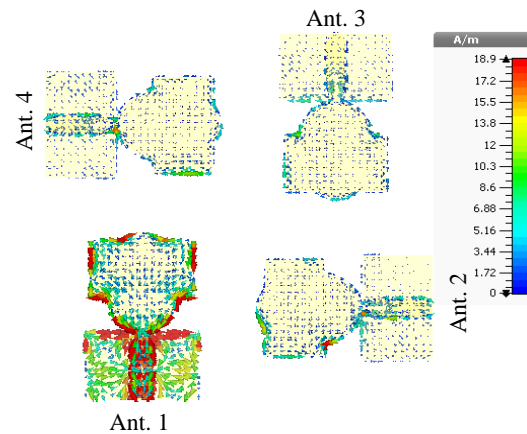

Figure 6. The simulated current distribution of SWB MIMO system at.

5. Results

The optimal MIMO system was fabricated to confirm the numerical simulation outcomes, and to showcase its applicability for 5G systems. The fabricated prototype is shown in the inset of Figure 7. Measurements of the reflection and transmission coefficients were performed using the Anritsu vector network analyzer MS4644B (0–40 GHz). The radiation patterns were validated in the anechoic chamber, as depicted in Figure 7. It is important to note that the measurements of the reflection coefficient, mutual coupling, and gain

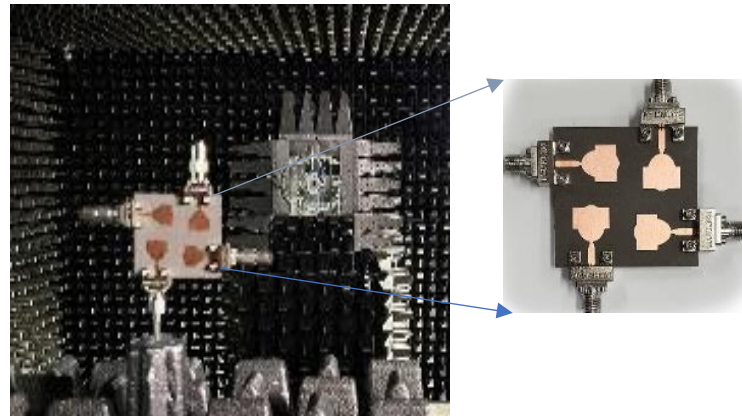were limited to 40 GHz, as the measurement range of the MS4644B VNA device used only extends up to 40 GHz.

Figure 7. The MIMO antenna in the anechoic chamber. The inset shows a magnified picture of the fabricated prototype.

Figures 8 and 9 illustrate the comparison between the simulated, measured $|S_{11}|$, and mutual couplings $|S_{21}|$, $|S_{21}|$, and $|S_{21}|$. The developed SWB MIMO provided a wide impedance bandwidth ranging from 3.4 to 70 GHz, effectively covering the all 5G bands. One can observe an acceptable match between both datasets using MS4644B VNA, which has a measurement range that extends up to 40 GHz. However, there is a noticeable difference between the measured and simulated data, particularly at higher frequencies. This is attributed to several factors, such as fabrication tolerances, cable loss, inaccuracies in assembly, and the utilization of large end-launch connectors.
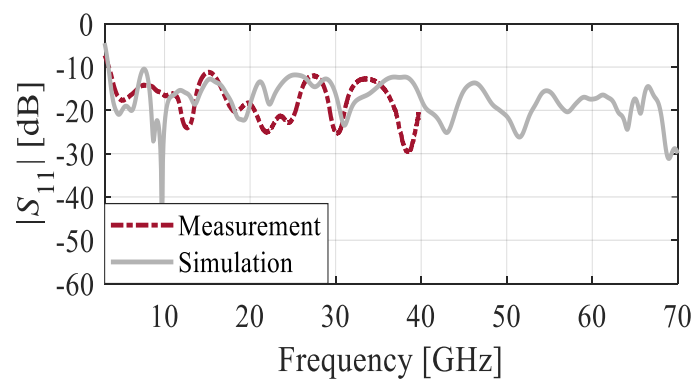

Figure 8. Simulated and measured reflection coefficients at Port 1.

The measured isolation between the four ports, $|S_{21}|$, $|S_{21}|$, and $|S_{21}|$, shows a strong resemblance to the simulation, thus validating that SWB MIMO offers an isolation of better than 20 dB across the entire range, cf. (Figure 9). Figure 10 displays the MIMO's simulated and measured maximum realized gain plots when exciting Port 1 and terminating the remaining ports with a 50-Ω load. As previously stated, the measurements were conducted up to 40 GHz using the VNA available in our laboratory. Nonetheless, the trends observed in the measured gain results suggest that the results beyond 40 GHz could also be favorable. The average gain of the n system was approximately 7 dB up to 44 GHz, and it exceeded 10 dB beyond 50 GHz.
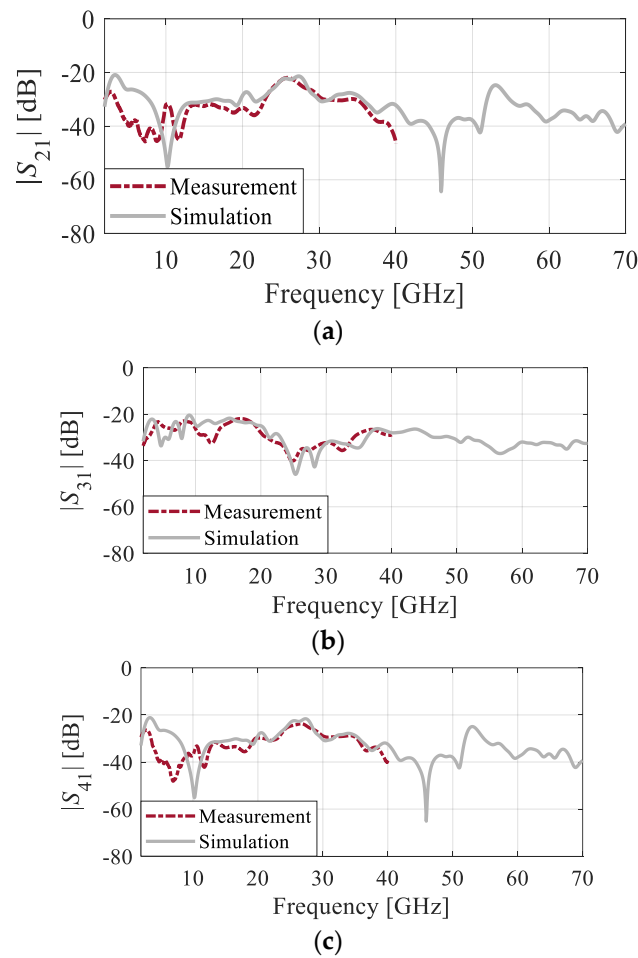
Figure 9. Transmission coefficients: simulations and measurements, (**a**) S_{21}, (**b**) S_{31}, and (**c**) S_{41}.
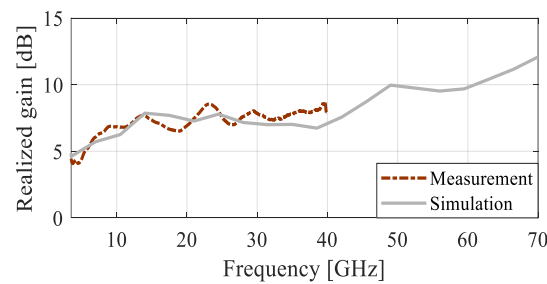
Figure 10. Simulated and measured realized gain at Port 1.

There is good matching between the two datasets, although a minor discrepancy is observed. This discrepancy may be explained, as previously, by inaccuracies pertaining to manufacturing; the other reasons may include imprecise assembly of the antenna or inaccurate angular placement of the antenna in the chamber. The E-plane and H-plane radiation patterns at 3.5 GHz, 10 GHz, 20 GHz, 28 GHz, 38 GHz, 45 GHz, and 65 GHz are shown in Figure 11a–g, where the measured and simulated results at Port 1are presented. The measured results are available for the initial five frequencies up to 40 GHz, as constrained by the mentioned measurement limitations. Conversely, simulated radiation results at 45 GHz and 65 GHz are provided to offer a more comprehensive perspective on radiation across the entire bandwidth. The radiation patterns at 3.5 GHz display bidirectional and omnidirectional characteristics in the E-plane and H-plane, respectively, with a low level of cross-polarized fields. At 10 GHz and 20 GHz, the MIMO system maintained low cross-polarization levels. However, at higher frequencies, both the E-plane and H-plane exhibit

distorted omnidirectional patterns and high cross-polarization levels due to the excitation of higher order modes.
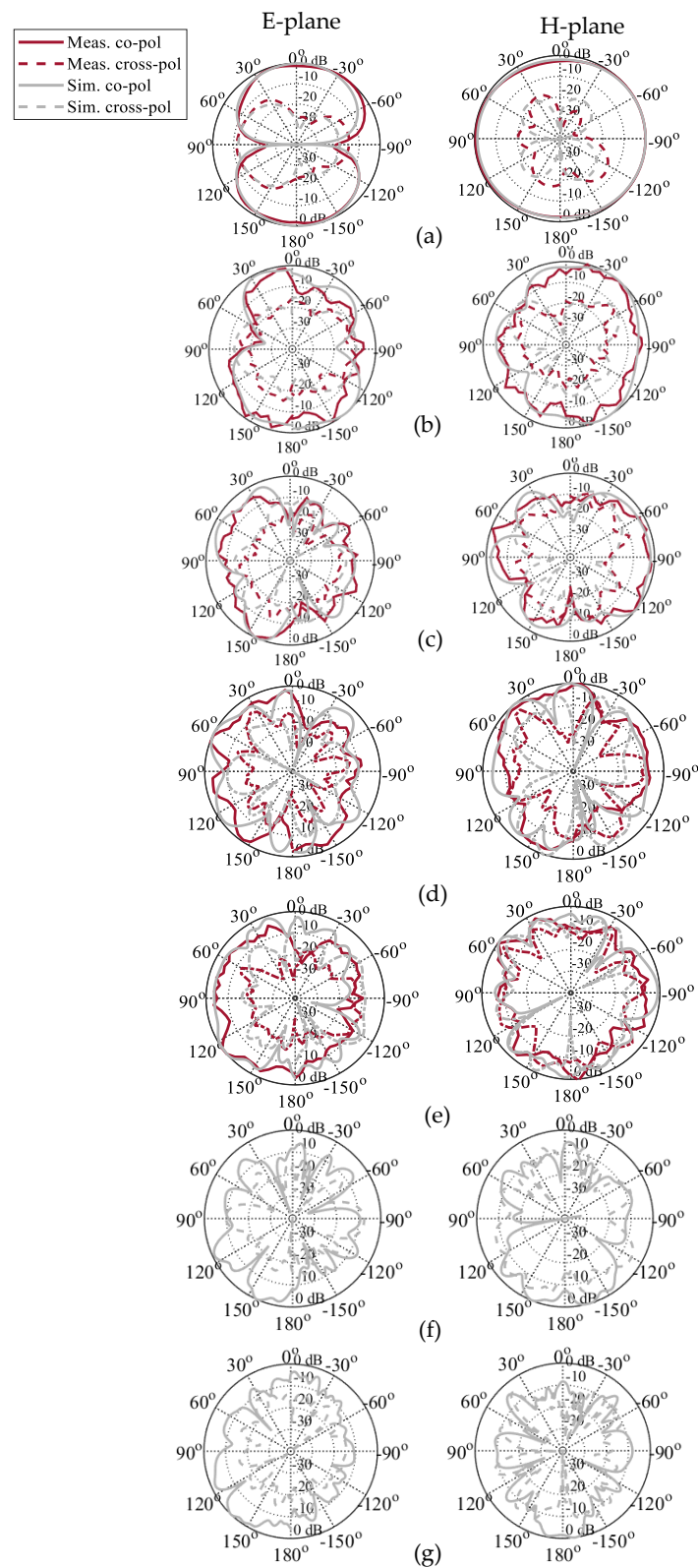

Figure 11. Simulated and measured radiation patterns of the SWB MIMO system in the E- and H-planes at Port 1, (**a**) 3.5 GHz, (**b**) 10 GHz, (**c**) 20 GHz, (**d**) 28 GHz, (**e**) 38 GHz, (**f**) 45 GHz, and (**g**) 65 GHz.

6. MIMO Performance

To evaluate the performance of a system, it is crucial to consider the correlation between MIMO ports. In this study, the four-element SWB MIMO system was analyzed using various parameters, including envelope correlation coefficient (ECC), diversity gain (DG), total active reflection coefficient (TARC), and channel capacity loss (CCL). These parameters were used to assess the system's reliability. ECC measures the correlation between MIMO elements, with an ideal value of zero, and a practical limit of below 0.5 [29,30]. It can be determined from the *S*-parameters as [31]

$$ECC_{ij} = \frac{\left| S_{ii}^* S_{ij} + S_{ji}^* S_{jj} \right|^2}{\left(1 - \left(|S_{ii}|^2 + |S_{ji}|^2\right)\right)\left(1 - \left(|S_{jj}|^2 + |S_{ij}|^2\right)\right)} \tag{6}$$

where ECC_{ij} indicates the correlation between the *i*th and *j*th MIMO elements. The simulated and measured ECC plots of the developed SWB MIMO system are shown in Figure 12a. The ECC is <3×10^{-3} for the entire bandwidth, satisfying the wireless network requirement (ECC < 0.5) [32]. The difference observed between the simulated and measured ECC can be attributed to the previously mentioned inconsistency in the simulation and measurement S-parameters. The DG, which shows the degree of transmission power reduction, constitutes an important performance metric. It is computed from the ECC as follows [33]

$$DG = 10 \times \sqrt{1 - \left| ECC_{ij} \right|^2} \tag{7}$$

(a)

(b)
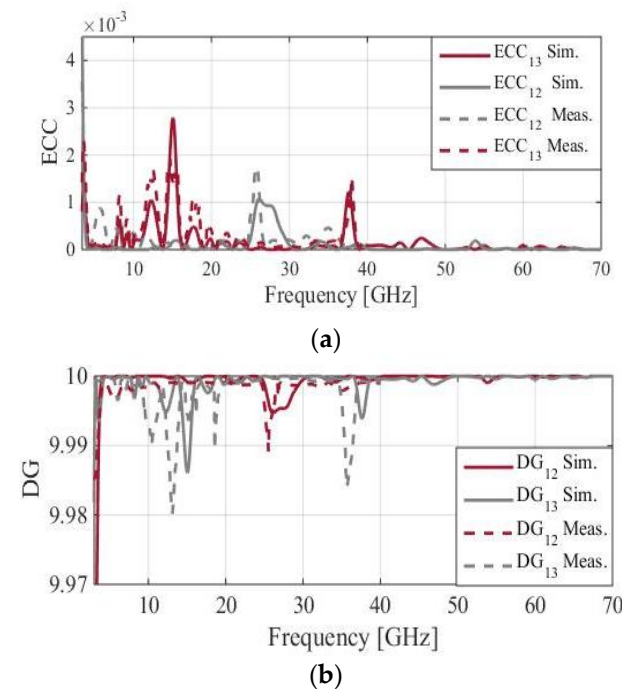
Figure 12. The diversity performance of the MIMO system; simulated and measured (**a**) ECC and (**b**) DG.

In general, higher DG values indicate better MIMO performance. Figure 12b presents the simulated and measured DG results, which show high DG values across the entire bandwidth, approaching the standard of 10 dB. Another crucial factor in evaluating the MIMO performance is TARC, which is defined as the ratio of the square root of the total reflected power to the square root of the total incident power. It is used to identify the

operating bands of a MIMO antenna as well as radiation performance when modifying the phase of the input signal. The TARC can be calculated using the following expression [34]:

$$TARC = \sqrt{\sum_{i=1}^{4} \left| S_{i1} + \sum_{n=2}^{4} S_{in} e^{j\theta_{n-1}} \right|^2 / 2} \tag{8}$$

$$TARC = \sqrt{\frac{\begin{array}{l} \left| S_{11} + S_{12}e^{j\theta_1} + S_{13}e^{j\theta_2} + S_{14}e^{j\theta_3} \right|^2 \\ + \left| S_{21} + S_{22}e^{j\theta_1} + S_{23}e^{j\theta_2} + S_{24}e^{j\theta_3} \right|^2 \\ + \left| S_{31} + S_{32}e^{j\theta_1} + S_{33}e^{j\theta_2} + S_{34}e^{j\theta_3} \right|^2 \\ + \left| S_{41} + S_{42}e^{j\theta_1} + S_{43}e^{j\theta_2} + S_{44}e^{j\theta_3} \right|^2 \end{array}}{4}} \tag{9}$$

where θ_i refers to excitation phase angle of the *i*th signal. Figure 13a depicts the simulated and measured TARC plots, indicating values of ≤ -10 dB across the entire bandwidth [35]. This provides additional evidence of the proposed system's SWB characteristic. The CCL is another essential parameter to assess the performance of MIMO systems, which quantifies channel capacity losses. The following equations can be used to calculate it [36]:

$$CCL = -log_2 \det(A) \tag{10}$$

where A is the correlation matrix,

$$A = \begin{bmatrix} \rho_{11} & \rho_{12} \\ \rho_{21} & \rho_{22} \end{bmatrix} \tag{11}$$

$$\rho_{ii} = 1 - \sum_{j=1}^{2} |S_{ij}|^2 \tag{12}$$

$$\rho_{ij} = -\left(S_{ii}^* S_{ij} + S_{ij} S_{ji}^* \right) \tag{13}$$
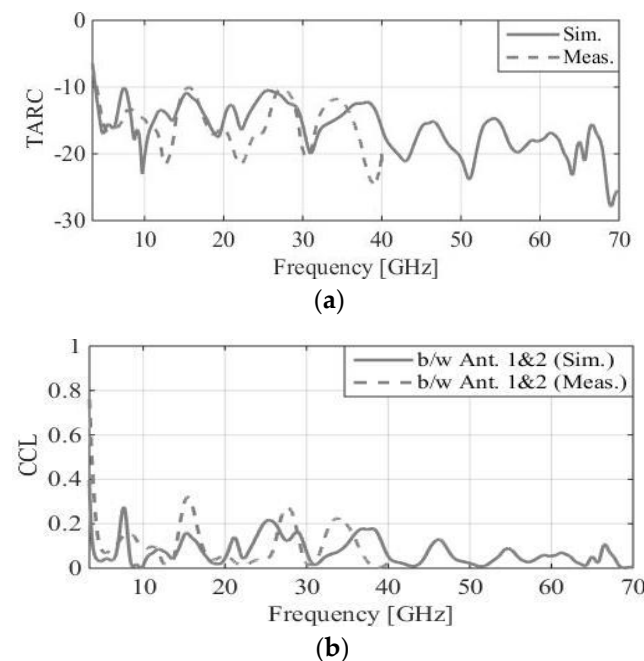

(a)

(b)

Figure 13. The simulated and measured (**a**) TARC and (**b**) CCL of the SWB MIMO system.

Figure 13b shows the simulated and measured CCL results, which indicate values lower than the established standard of 0.4 bit/s/Hz. These values are lower than the

practical standard of 0.4 bit/s/Hz [37]. The proposed system demonstrates excellent diversity performance, as indicated by the low ECC ($<3 \times 10^{-3}$), TARC (≤ -10 dB), and CCL (<0.3 bit/s/Hz) values, as well as the high DG (≈ 10 dB) across the entire bandwidth. These results are indicative of the suitability of the system for transmission systems featuring a high data rate.

Table 1 presents a performance comparison between the proposed SWB MIMO and the state-of-the-art structures reported in the recent literature. In contrast to previous findings, the SWB MIMO antenna developed in this work demonstrates the highest isolation and bandwidth. Importantly, these properties are achieved without employing any decoupling techniques that could have increased the system's size and complexity. Additionally, it features a compact and low-profile design, high gain, and excellent diversity performance.

Table 1. Comparison between the developed SWB MIMO system and state-of-the-art structures.

Ref.	Single Antenna Structure (Size λ^2_{max}) (Substrate)	BW Range (GHz)	BW Enhance Method	Max.(Min.) Gain (dB)	Isolation (dB)	Cross-Polarization Level	ECC DG (dB) CCL (bits/s/H)		Decoupling Structure
[11]	Bow tie (0.25 × 0.2) (FR-4)	3.035–17.39	Using CPW feed	6.16 (2)	—	—		—	—
[12]	Monople antenna (0.2 × 0.21) (Rogers RT5880	2.11–70	Using DGS	8.15 (2.4)	—	<12 dB at 27.95 GHz and 0° direction		—	—
[13]	S-shaped monopole (0.36 × 0.36) (Rogers RT5880)	3.08–40.9	Using DGS	5.9 (1.8)	—	—		—	—
[15]	Monopole antenna (0.21 × 0.28) (FR-4)	1.8–30	Include slots	5 (3.5)	—	—		—	—
[17]	Spade-shaped antenna (0.29 × 0.22) (FR-4)	3–40	Utlizing DGS and slot	12 (4.4)	>17	—	- (<0.04) - (>9.5) - (<0.6)		Windmill shape
[18]	Yagi antenna (0.2 × 0.25) (FR-4)	1.37–16	Using diamond shaped and flared reflector	5.4 (3.5)	>16	<20 dB at 15.6 GHz and maximum direction	- (<0.01) - (——) - (——)		Self decoupling
[19]	Feather-shaped antenna (0.45 × 45) (FR-4)	4.4–51.5	Include slots and notches	—	>15	—	- (<0.1) - (——) - (<0.4)		Diagonal strip as an interelement separation
This work	Elliptical-square monopole (0.226 × 0.226) (Rogers RT5880)	3.4–70	Combine both shapes and employ optimization technique	12 (6)	>20	<19 dB at 27.95 GHz and 0° direction	- (<3 × 10^{-3}) - (>9.99) - (<0.3)		Self decoupling

λ_{max} refers to free space wavelength corresponding to the minimum frequency of the band.

A compact self-decoupling MIMO on single-layer Rogers PCB with SWB, and high isolation and gain properties for 5G microwave and mm-wave applications, was developed. The proposed antenna design utilizes a simple elliptical-square structure that combines these two shapes to achieve SWB spanning from 3.4 GHz to 70 GHz. The antenna is capable of covering 5G frequency bands at 3.5, 26, 28, 38, 50, and 60 GHz. A gradient-based algorithm with numerical derivatives and design-goal regularization was utilized for antenna parameter refinement and simultaneously ensured SWB and high gain.

7. Conclusions

Afterwards, the MIMO system was implemented with four radiators arranged orthogonally. This configuration helps to lower the mutual coupling to below -20 dB in the entire

bandwidth. Further, it provides a high gain that exceeds 10 dB beyond 50 GHz and reaches a maximum of 12 dB at 70 GHz. The system displays excellent diversity performance, which is confirmed by the low ECC, TARC, and CCL metrics, along with the high DG values. The developed SWB MIMO system was experimentally validated. Good agreement between the simulated and measured data was observed. Overall, the proposed design provides a compact, low-cost, low-profile system of lower complexity featuring high isolation and gain, and a very-broad bandwidth in comparison to the state-of-the-art designs.

Author Contributions: Conceptualization, methodology, and software, B.A.F.E. and S.K.; formal analysis and investigation, B.A.F.E.; validation, B.A.F.E. and S.K.; visualization, B.A.F.E. and A.P.-D.; writing—original draft preparation, B.A.F.E.; writing—review and editing, S.K. and A.P.-D.; supervision, S.K.; project administration, S.K.; funding acquisition, S.K. and A.P.-D.; resources, S.K. All authors have read and agreed to the published version of the manuscript.

Data Availability Statement: Data are contained within the article.

Conflicts of Interest: The authors declare no conflict of interest.

References

1. Wang, C.-X.; You, X.; Gao, X.; Zhu, X.; Li, Z.; Zhang, C.; Wang, H.; Huang, Y.; Chen, Y.; Haas, H.; et al. On the road to 6G: Visions, Requirements, key technologies, and testbeds. *IEEE Comm. Surv. Tutor.* **2023**, *25*, 905–974. [CrossRef]
2. Ullah, H.; Abutarboush, H.F.; Rashid, A.; Tahir, F.A. A compact low-profile antenna for Millimeter-Wave 5G mobile phones. *Electronics* **2022**, *11*, 3256. [CrossRef]
3. Esmail, B.A.F.; Majid, H.B.; Dahlan, S.H.; Abidin, Z.Z.; Rahim, M.K.A.; Jusoh, M. Planar antenna beam deflection using low-loss metamaterial for future 5G applications. *Int. J. RF Microw. Comput. Aided Eng.* **2019**, *29*, e21867. [CrossRef]
4. Li, J.; Matos, C.; Ghalichechian, N. A low-cost vertically integrated antenna array at 60 GHz with 85% efficiency. *IEEE Antennas Wirel. Propag. Lett.* **2021**, *20*, 513–517. [CrossRef]
5. Esmail, B.A.; Koziel, S. Design and optimization of metamaterial-based dual-band 28/38 GHz 5G MIMO antenna with modified ground for isolation and bandwidth improvement. *IEEE Antennas Wirel. Propag. Lett.* **2023**, *22*, 1069–1073. [CrossRef]
6. Ancans, G.; Bobrovs, V.; Ancans, A.; Kalibatiene, D. Spectrum considerations for 5G mobile communication systems. *Proc. Comput. Sci.* **2017**, *104*, 509–516. [CrossRef]
7. Li, C.; Huang, Y.; Li, S.; Chen, Y.; Jalaian, B.A.; Hou, Y.T.; Lou, W.; Reed, J.H.; Kompella, S. Minimizing AoI in a 5G-based IoT network under varying channel conditions. *IEEE Internet Things J.* **2021**, *8*, 14543–14558. [CrossRef]
8. Attia, H.; Abdalrazik, A.; Sharawi, M.S.; Kishk, A.A. Wideband circularly-polarized Millimeter-Wave DRA array for Internet of Things. *IEEE Internet Things J.* **2023**, *10*, 9597–9606. [CrossRef]
9. Pfeiffer, C.; Massman, J. A UWB low-profile hemispherical array for wide angle scanning. *IEEE Trans. Antennas Propag.* **2023**, *71*, 508–517. [CrossRef]
10. Sim, C.-Y.-D.; Lo, J.-J.; Chen, Z.N. Design of a broadband millimeter-wave array antenna for 5G applications. *IEEE Antennas Wirel. Propag. Lett.* **2023**, *22*, 1030–1034. [CrossRef]
11. Azim, R.; Islam, M.T.; Arshad, H.; Alam, M.M.; Sobahi, N.; Khan, A.I. CPW-fed super-wideband antenna with modified vertical bow-tie-shaped patch for wireless sensor networks. *IEEE Access* **2020**, *9*, 5343–5353. [CrossRef]
12. Ayyappan, M.; Patel, P. On design of a triple elliptical super wideband antenna for 5G applications. *IEEE Access* **2022**, *10*, 76031–76043. [CrossRef]
13. Ullah, S.; Ruan, C.; Sadiq, M.S.; Haq, T.U.; Fahad, A.K.; He, W. Super wide band, defected ground structure (DGS), and stepped meander line antenna for WLAN/ISM/WiMAX/UWB and other wireless communication applications. *Sensors* **2020**, *20*, 1735. [CrossRef] [PubMed]
14. Kundu, S.; Chatterjee, A. A compact super wideband antenna with stable and improved radiation using super wideband frequency selective surface. *AEU Int. J. Electron. Commun.* **2022**, *150*, 154200. [CrossRef]
15. Lazović, L.; Jokanovic, B.; Rubežić, V.; Radovanovic, M.; Jovanović, A. Fractal cardioid slot antenna for Super Wideband Applications. *Electronics* **2022**, *11*, 1043. [CrossRef]
16. Jayant, S.; Srivastava, G. Close-packed quad-element triple band-notched UWB MIMO antenna with upgrading capability. *IEEE Trans. Antennas Propag.* **2023**, *71*, 353–360. [CrossRef]
17. Yu, C.; Yang, S.; Chen, Y.; Wang, W.; Zhang, L.; Li, B.; Wang, L. A super-wideband and high isolation MIMO antenna system using a windmill-shaped decoupling structure. *IEEE Access* **2020**, *8*, 115767–115777. [CrossRef]
18. Chaudhari, A.D.; Ray, K.P. A single-layer compact four-element quasi-Yagi MIMO antenna design for super-wideband response. *AEU Int. J. Electron. Commun.* **2021**, *138*, 153878. [CrossRef]
19. Singhal, S. Feather-shaped super wideband MIMO antenna. *Int. J. Microw. Wirel. Technol.* **2021**, *13*, 94–102. [CrossRef]

20. Akgiray, A.; Weinreb, S.; Imbriale, W.A.; Beaudoin, C. Circular quadruple-ridged flared horn achieving near-constant beamwidth over multioctave bandwidth: Design and measurements. *IEEE Trans. Antennas Propag.* **2013**, *61*, 1099–1108. [CrossRef]

21. Abdalmalak, K.A.; Romano, S.L.; García, E.; Lampérez, A.G.; Martínez, F.J.; Palma, M.S.; Vargas, D.S.; Puente, J.M.; Tercero, F.; Pérez, J.A.; et al. Radio astronomy ultra wideband receiver covering the 2–14 GHz frequency band for VGOS applications. In Proceedings of the 2016 10th European Conference on Antennas and Propagation (EuCAP), Davos, Switzerland, 10–15 April 2016; pp. 1–5.

22. Yang, J.; Pantaleev, M.; Kildal, P.-S.; Klein, B.; Karandikar, Y.; Helldner, L.; Wadefalk, N.; Beaudoin, C. Cryogenic 2–13 GHz Eleven feed for reflector antennas in future wideband radio telescopes. *IEEE Trans. Antennas Propag.* **2011**, *59*, 1918–1934. [CrossRef]

23. Siddiqui, J.Y.; Saha, C.; Sarkar, C.; Shaik, L.A.; Antar, Y.M.M. Ultra-wideband antipodal tapered slot antenna with integrated frequency-notch characteristics. *IEEE Trans. Antennas Propag.* **2018**, *66*, 1534–1539. [CrossRef]

24. Dey, S.; Karmakar, N.C. Design of novel super wide band antenna close to the fundamental dimension limit theory. *Sci. Rep.* **2020**, *10*, 16306. [CrossRef] [PubMed]

25. Koziel, S.; Pietrenko-Dabrowska, A.; Mahrokh, M. On decision-making strategies for improved-reliability size reduction of microwave passives: Intermittent correction of equality constraints and adaptive handling of inequality constraints. *Knowl. Based Syst.* **2022**, *255*, 109745. [CrossRef]

26. Koziel, S.; Pietrenko-Dabrowska, A. Reliable EM-driven size reduction of antenna structures by means of adaptive penalty factors. *IEEE Trans. Antennas Propag.* **2021**, *70*, 1389–1401. [CrossRef]

27. Conn, A.R.; Gould, N.I.; Toint, P.L. Trust Region Methods. In *MPS-SIAM Series on Optimization*; Society for Industrial and Applied Mathematics: Philadelphia, PA, USA, 2000.

28. Levy, H.; Lessman, F. *Finite Difference Equations*; Dover Publications Inc.: New York, NY, USA, 1992.

29. Esmail, B.A.; Koziel, S. High isolation metamaterial-based dual-band MIMO antenna for 5G millimeter-wave applications. *AEU Int. J. Electron. Commun.* **2023**, *158*, 154470. [CrossRef]

30. Dash, J.C.; Kharche, S.; Reddy, G.S. MIMO antenna mutual coupling reduction using modified inverted-fork shaped structure. *IEEE Can. J. Electr. Comput. Eng.* **2022**, *45*, 375–382. [CrossRef]

31. Liu, K.; Li, Z.; Cui, W.; Zhang, K.; Wang, M.; Fan, C.; Zheng, H.; Li, E. Investigation of conformal MIMO antenna for implantable devices based on theory of characteristic modes. *IEEE Trans. Antennas Propag.* **2022**, *70*, 11324–11334. [CrossRef]

32. Suresh, A.C.; Reddy, T.S.; Madhav, B.T.P.; Das, S.; Lavadiya, S.; Algarni, A.D.; El-Shafai, W. Investigations on stub-based uwb-mimo antennas to enhance isolation using characteristic mode analysis. *Micromachines* **2022**, *13*, 2088. [CrossRef]

33. Güler, C.; Bayer Keskin, S.E. A novel high isolation 4-Port compact MIMO antenna with DGS for 5G applications. *Micromachines* **2023**, *14*, 1309. [CrossRef]

34. Wu, A.; Tao, Y.; Zhang, P.; Zhang, Z.; Fang, Z. A compact high-isolation four-element MIMO antenna with asymptote-shaped structure. *Sensors* **2023**, *23*, 2484. [CrossRef] [PubMed]

35. Biswas, A.K.; Pattanayak, S.S.; Chakraborty, U. Evaluation of dielectric properties of colored resin plastic button to design a small MIMO antenna. *IEEE Trans. Instrum. Meas.* **2020**, *69*, 9170–9177. [CrossRef]

36. Abdulkawi, W.M.; Malik, W.A.; Rehman, S.U.; Aziz, A.; Sheta, A.F.A.; Alkanhal, M.A. Design of a compact dual-band MIMO antenna system with high-diversity gain performance in both frequency bands. *Micromachines* **2021**, *12*, 383. [CrossRef] [PubMed]

37. Hussain, R.; Alreshaid, A.T.; Podilchak, S.K.; Sharawi, M.S. Compact 4G MIMO antenna integrated with a 5G array for current and future mobile handsets. *IET Microw. Antennas Propag.* **2017**, *11*, 271–279. [CrossRef]